Materials Today Bio 26 (2024) 101105

Contents lists available at ScienceDirect

Materials Today Bio

journal homepage: www.journals.elsevier.com/materials-today-bio

An artificial signaling pathway primitive-based intelligent biomimetic nanoenzymes carrier platform for precise treatment of Her2 (+) tumors

Yuliang Sun [a,b,c,1], Wenlong Zhang [a,1], Yilin Lu [a], Yanan He [a], Badrul Yahaya [b,c,***], Yanli Liu [a,**], Juntang Lin [a,*]

[a] Stem Cell and Biotherapy Technology Research Center, Henan Joint International Research Laboratory of Stem Cell Medicine, Xinxiang Medical University, Xinxiang, 453003, China

[b] Department of Biomedical Sciences, Advanced Medical and Dental Institute (IPPT), Universiti Sains Malaysia, SAINS@BERTAM, 13200, Kepala Batas, Penang, Malaysia

[c] Breast Cancer Translational Research Program (BCTRP), Advanced Medical and Dental Institute, Universiti Sains Malaysia, Bertam, 13200, Kepala Batas, Pulau Pinang, Malaysia

ARTICLE INFO

Keywords:
$MSC^{intelligent}$
Her2 (+) tumor
Intelligent modification
Artificial signaling pathway
Nanoenzymes

ABSTRACT

In tumor treatment, the deposition of nanoenzymes in normal tissues and cause potential side effects are unavoidable. Here, we designed an intelligent biomimetic nanoenzymes carrier platform ($MSC^{intelligent}$) that endows the carrier platform with "wisdom" by introducing Affibody-Notch(core)-VP64-GAL4/UAS-HSV-TK artificial signal pathways to mesenchymal stem cells (MSCs). This intelligent nanoenzymes carrier platform is distinguished from the traditional targeting tumor microenvironment or enhancing affinity with tumor, which endue $MSC^{intelligent}$ with tumor signal recognition capacity, so that $MSC^{intelligent}$ can autonomously distinguish tumor from normal tissue cells and feedback edited instructions. In this study, $MSC^{intelligent}$ can convert tumor signals into HSV-TK instructions through artificial signal pathway after recognizing Her2 (+) tumor. Subsequently, the synthesized HSV-TK can rupture $MSC^{intelligent}$ under the mediation of ganciclovir, and release the preloaded Cu/Fe nanocrystal clusters to kill the tumor accurately. Meanwhile, $MSC^{intelligent}$ without recognizing tumors will not initiate the HSV-TK instructions, thus being unresponsive to GCV and blocking the release of nanoenzymes in normal tissues. Consequently, $MSC^{intelligent}$ is the first intelligent biomimetic nanoenzymes carrier platform, which represents a new biomimetic nanoenzymes targeting mode.

1. Introduction

Patients with Her2 (+) tumors are characterized by poor prognosis, high mortality, and poor sensitivity to chemotherapy drugs, which seriously affects their survival and quality of life. In recent years, nanoenzymes-initiated nanomedicine has attracted extensive attention in tumor treatment. Whether based on the endogenous responsiveness of the tumor microenvironment (pH [1], GSH [2], ROS [3], etc.) or the exogenous responsiveness of magnetic fields [4]and phototherapy [5,6], nanoenzymes have exhibited promising therapeutic potential. However, although the enhanced permeability and retention (EPR) effect can effectively promote the enrichment of nanoenzymes at the tumor site, such enrichment still cannot reach 1 % of the total nanoparticles [7,8]. Currently, many targeted modification strategies for nanoenzymes can improve their enrichment in tumors, but most nanoparticles cannot reach the tumor site because of the unique characteristics of the human physiological structure. These nanoparticles deposited in normal tissues are often phagocytized by macrophages in the reticuloendothelial system and eventually accumulate in normal organs, such as the liver and spleen, for a long time and directly interact with normal tissues, which inevitably causes long-term injury, fibrosis, and even cancer [9,10].

Although the existing biomimetic nanoenzymes carrier platforms

* Corresponding author.
** Corresponding author.
*** Corresponding author. Department of Biomedical Sciences, Advanced Medical and Dental Institute (IPPT), Universiti Sains Malaysia, SAINS@BERTAM, 13200, Kepala Batas, Penang, Malaysia.
E-mail addresses: badrul@usm.my (B. Yahaya), liuyanli198512@163.com (Y. Liu), linjtlin@126.com (J. Lin).
[1] These authors contributed equally to this work.

https://doi.org/10.1016/j.mtbio.2024.101105
Received 23 January 2024; Received in revised form 3 May 2024; Accepted 27 May 2024
Available online 1 June 2024

such as cells [11], bacteria [12], and cell membranes [13–15] can effectively block the interaction between nanoenzymes and normal tissues in vivo and reduce nanoenzymes-induced toxicity on normal tissues. However, this strategy also simultaneously blocks the contact between nanoenzymes and tumor tissue or tumor microenvironment and weakens the killing effect of nanoenzymes on the tumor. Furthermore, the majority of design strategies of these biological nanoenzymes carrier platforms mainly focus on targeting the tumor microenvironment or increasing the affinity with the tumor, which indeed partly improves the enrichment of nanoenzymes in tumors. However, due to these biomimetic functional nanoenzymes not having pre-set intelligence, they rely on natural homing to identify tumors. But the original function of receptors in natural live cell carriers is not to recognize tumors, so they may not be able to accurately distinguish tumor signals from other lesion microenvironments, resulting in off target. And this homing effect that deviates from its original physiological function is usually weak. We posit that an ideal modification strategy of the nanoenzymes is supposed to endow them with "wisdom" and make them precisely recognize/distinguish cancer cells from normal tissue cells and exclusively deliver drugs to tumor sites after making judgments.

To achieve the abovementioned objectives, we endue intelligent modification to menstrual blood-derived endometrial stem cells (MenSC) through gene editing, customized a Her2 (+) tumor cell artificial recognition receptor and the corresponding signal feedback structure for MSCs, and combined with nanoenzymes (Cu/Fe nanocrystal clusters) to constructed an intelligent biomimetic nanoenzymes carrier platform ($MSC^{intelligent}$). This biomimetic nanoenzymes carrier platform can truly recognize and distinguish Her2 (+) tumor and normal human tissue cells according to the internal intelligent artificial DNA program (artificial signaling pathway) to realize the accurate/exclusive release of nanoenzymes to tumor sites (Fig. 1). Additionally, compared to other types of mesenchymal stem cells (MSCs), MenSCs is more primitive, exhibits superior proliferation capacity and non-tumorigenic potential [16–18]. Therefore, MenSCs could be taken as an excellent stem cell source for creating intelligent biomimetic nanozyme carrier platforms.

Notch protein is an evolutionarily highly conserved cell membrane surface receptor, which can regulate the development of biological cells by recognizing notch ligand (DSL protein) [19]. Previous studies have shown that Notch protein can still perform notch-like functions by retaining only the smallest transmembrane core domain even though replacing intracellular and extracellular domains [20–23]. Based on this characteristic, this study used Her2-specific antigen receptor (affibody) and VP64 to replace the extracellular and intracellular domains of Notch protein, respectively, to create an artificial receptor that can recognize Her2 (+) tumors and connected the Her2 (+) tumor receptor and thymidine kinase (HSV-TK) signal feedback structure through the GAL4/UAS gene expression regulation system to construct the intelligent artificial signaling pathway to recognize tumors. Because Her2 (+) tumors are different from normal tissues in that they highly express the Her2 protein, the artificial signaling pathway (Affibody-Notch(core)-VP64-GAL4/UAS-HSV-TK) equipped in $MSC^{intelligent}$ can help MSCs intelligently distinguish Her2 (+) tumors and normal tissues by recognizing the Her2 protein expressed on tumor cells. Once the Her2 protein expressed on tumor cells is recognized by the recognition structure of $MSC^{intelligent}$, VP64 will transmit a tumor signal to activate the GAL4/UAS gene expression regulatory element and specifically initiate the expression of the HSV-TK gene in the response structure. Then, the expressed HSV-TK can convert ganciclovir (GCV), a conventional low toxicity for the clinical treatment of herpes, into ganciclovir triphosphate (GCV-TP), which inhibits DNA replication and results in the rupture of $MSC^{intelligent}$ and release of nanoenzymes. Simultaneously, because of the lack of a Her2 protein stimulation signal in normal tissues, $MSC^{intelligent}$ will default these cells as normal tissue cells and not activate the coupled artificial signaling pathway and HSV-TK gene expression. Due to the low toxicity of GCV, even in the presence of GCV,

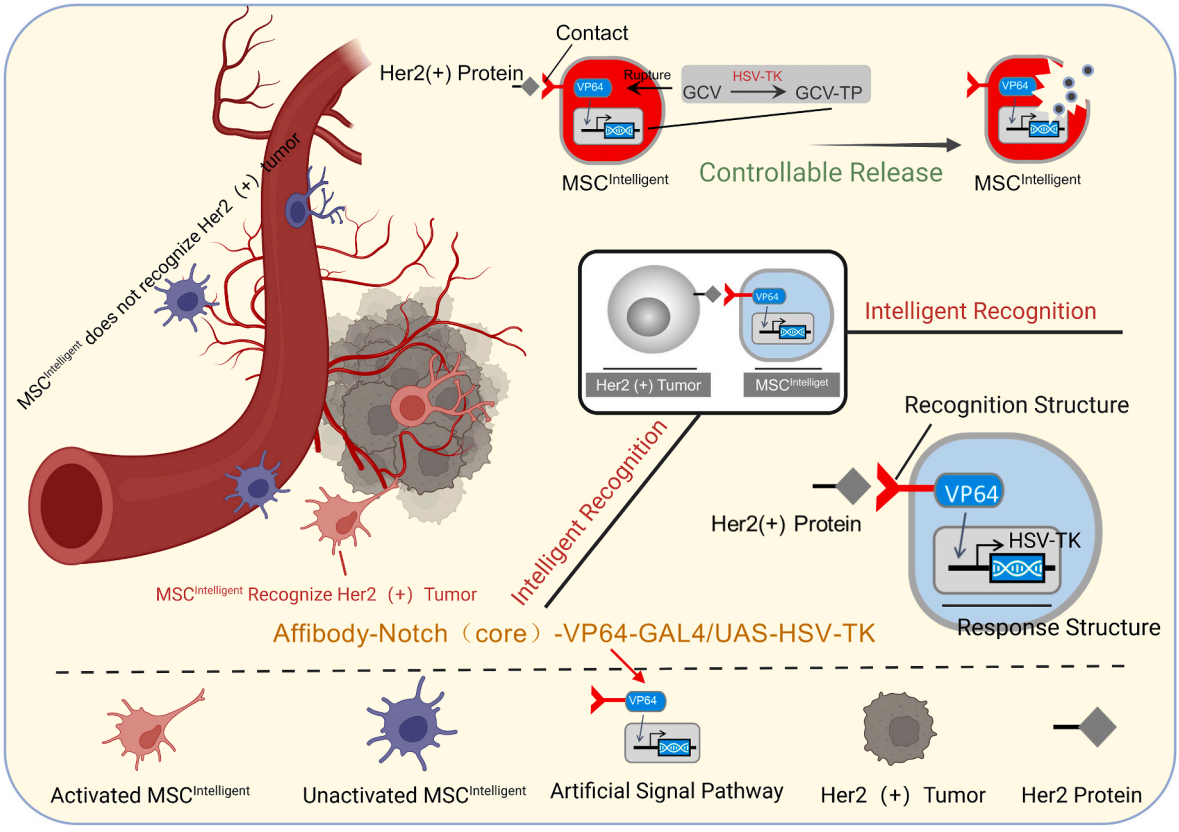

Fig. 1. $MSC^{intelligent}$'s process and principle for intelligent recognition of Her2 (+) tumors.

$MSC^{intelligent}$ will not be ruptured and release nanoenzymes (Fig. 1). Based on the intelligent recognization of $MSC^{intelligent}$ to Her2 (+) tumors and the unique artificial signaling pathway, $MSC^{intelligent}$ can not only perform the accurate release of nanoenzymes in the tumor site but also effectively block the release of nanoenzymes in normal tissue. Consequently, this is the first intelligent biomimetic nanoenzymes carrier platform that can autonomously distinguish tumors from normal tissue cells by the intelligent system (artificial signaling pathways), which provides a new alternative for the application of nanoenzymes in tumor therapy.

2. Materials and methods

2.1. Cells and animals

The MSCs used in this study are menstrual blood-derived endometrial stem cells, which are provided by Zhong yuan Stem Cell Research Institute of Xinxiang high tech Zone. All experimental procedures in this study were approved by the ethics committee of Xinxiang Medical University and carried out in accordance with the approved guidelines. Female BALB/c-nude mice and BALB/c mice aged 6–8 weeks (18–25 g) were purchased from Vital River Laboratories (Beijing, China; license No. SCXK (Beijing) 2016–0006). Mice were randomly divided into cages and housed in a specific pathogen-free environment with a temperature of 25 °C, a humidity of 50 ± 5 %, and a light-dark cycle of 12 h. All the treatment and laboratory procedures on mice were performed in accordance with the guidelines of the ethic committee of Xinxiang Medical University.

2.2. Establishment of $MSC^{intelligent}$ and fluorescence-labeled cells

The notch (core) in $MSC^{intelligent}$ originates from mouse Notch1 (nm_008714; Ile1427 to Arg1752). In order to label the recognition structure, we fused the c-myc tag (EQKLISEEDL) into the N-terminal of recognition structure and added the puromycin resistance tag. Simultaneously, the transcriptional activation sequence in the response structure contained five repeated GAL4 DBD targeting sequences (GGAGCACTGTCCTCCGAACG) and a BFP tag driven by independent promoter was added in the response structure. The recognition structure and response structure were integrated into the genome of MSCs by conventional lentivirus-mediated transfection. After stable expression, puromycin screening and flow cytometry sorting were consecutively performed. Additionally, Skov3, BT474, Svog, BJ, L02, and 293 T cells were labeled with GFP.

2.3. Immunofluorescence

Human breast cancer tissue: the sections were immersed in antigen repair solution at 90°C–100 °C, incubated in 100 °C water for 20 min, cooled naturally to room temperature, and washed three times with PBS. Subsequently, the slices were permeabilized with 0.5 % Triton X-100 at room temperature for 25 min and washed three times with PBS. After blocking with 10 % goat serum for 2 h, the samples were incubated with rabbit anti-human Her2 primary antibody (CY3086; Abways) in a wet box at 4 °C overnight. Then, the sections were incubated with Cy5-labeled Goat anti-rabbit IgG secondary antibody at 37 °C for 1 h, and the nuclei were stained with DAPI. Finally, the sections were observed and imaged under confocal microscopy.

$MSC^{intelligent}$: In accordance with the above procedures, Triton X-100 was used to permeabilize and goat serum to block the cells. Thereafter, the primary antibody (mouse-derived c-myc tag, AB0001; Abways) and the secondary antibody (FITC-labeled Goat anti-mouse IgG) was used to finish the subsequent immunofluorescent staining.

2.4. Synthesis and surface modification of Cu + -contained Cu/Fe nanocrystal clusters (CCFC)

Ferric chloride hexahydrate (FeCl3·6H2O), Copper (II) chloride dihydrate (CuCl2·2H2O), ethylene glycol (EG), and anhydrous sodium acetate (NaAc) were obtained from Sinopharm Chemical Reagent Co., Ltd. Polyvinyl pyrrolidone K30 (PVP) was purchased from Sigma-Aldrich. Bovine serum albumin (BSA) was bought from Aladdin Chemistry Co., Ltd. All chemicals listed above were of analytic grade or better. CCFC was prepared by a solvothermal reaction. Briefly, 1.62 g of FeCl3·6H2O, 0.51 g of CuCl2·2H2O, 3.28 g of NaAc, and 1.00 g PVP were dissolved in 40 mL of EG. The mixture was sealed in a Teflon-lined autoclave and kept at 200 °C for 12 h. After the reaction, the precipitate was collected by centrifugation and rinsed with water and ethanol several times, and then redispersed in water and exposed to air for 15 days. Finally, the product CCFC was collected and dried in a vacuum lyophilizer. For surface modification of BSA on CCFC, 20 mg of BSA was dispersed in 5 mL of CCFC aqueous solution (200 ppm) via ultrasonication at room temperature for 2 h. Next, we obtained the BSA-modified CCFC (CCFCB) by centrifugation, and being washed with deionized water three times to remove excessive BSA. At last, this CCFCB was dried in a vacuum lyophilizer and stored in an argon atmosphere glovebox for further application.

2.5. Characterization of CCFC

The images of CCFC prepared by the above one-step method were obtained by scanning electron microscope (s-4800), transmission electron microscope (jem-2100f), and high-resolution transmission electron microscope (HRTEM). Infrared spectrometer (Nicolet nexus670) collects Fourier transform infrared spectrum. XRD was detected by D/max-2550pc X-ray diffractometer (RIGAKU). Energy spectrum analyzer (EDS) obtains EDS mapping of Cu, Fe, and O element distribution of CCFC.

2.6. POD-like catalytic activity of CCFCB

The POD-like catalytic activity of CCFCB was examined by 3,3′,5,5′-tetramethylbiphenyl (TMB, purchased from Aladdin Chemistry Co., Ltd.) as the substrate in the presence of H_2O_2. CCFCB (2000 ppm) and TMB (15 mM) were added into 4.43 mL of PBS (pH = 5.5). The absorption peak of TMB (652 nm) was acquired by UV–visible spectra.

2.7. Loading capacity of CCFCB in $MSC^{intelligent}$

$MSC^{intelligent}$ was cultured in the cell culture dish for 12 h, and then, FITC-labeled CCFCB was added and incubated with $MSC^{intelligent}$ for 6 h and washed with PBS three times. A confocal microscope (Nikon) was used to observe the positional relationship between CCFCB and $MSC^{intelligent}$ from various angles based on three-dimensional reconstruction. Subsequently, the cells were fixed with 4 % paraformaldehyde (PFA) for 20 min, and the FITC-labeled cells were detected by flow cytometry.

Subsequently, $MSC^{intelligent}$ were cultured in 24-well plates overnight and incubated with CCFCB of 0 ppm, 10 ppm, 20 ppm, 30 ppm, and 40 ppm for 6 h. Excessive CCFCB was washed with PBS, and $MSC^{intelligent}$ was collected. After ultrasonication, $MSC^{intelligent}$ was centrifuged at 2000 g for 10min, excessive HCl solution (pH = 2) was added to dissolve CCFCB, and pH was adjusted to 7 with NaOH solution. After constant volume to 1 mL, the concentration of iron was quantified according to the tissue iron assay kit (BC4350; Solarbio). Using the same method to dissolve CCFCB and measure iron ion concentration, and plot the standard curve between CCFCB and iron ions. The iron ion concentration in the $MSC^{intelligent}$ mentioned above was converted into the amount of CCFCB using the standard curve.

2.8. Prussian blue staining

After being cultured overnight, $MSC^{intelligent}$ was incubated with 20 ppm CCFCB for 6 h, and the excessive CCFCB was washed with PBS. Then, the cells were fixed with 4 % PFA and stained according to the prussian blue iron staining kit (G1424; Solarbio).

2.9. Recognition of Her2 (+) tumor by $MSC^{intelligent}$

3×10^5 $MSC^{intelligent}$ were cocultured with 2×10^4 GFP-labeled Her2 (+) tumor cells (Skov3-GFP and BT474-GFP) or GFP-labeled normal tissue cells (Svog-GFP, BJ-GFP, L02-GFP, 293 T-GFP), respectively. The cell interactions were observed and imaged under a confocal microscope. Furthermore, three groups were set in the Transwell experiment, group A: $MSC^{intelligent}$ cells alone cultured in the lower layer; group B (Non-contact coculture): Skov3-GFP cells cultured in the upper layer and $MSC^{intelligent}$ in the lower layer; group C (Contact coculture): Skov3-GFP and $MSC^{intelligent}$ were mixed and cultured in the lower layer in. After being cultured for 48 h, the cell interactions were observed and imaged under confocal microscopy.

2.10. Rupture of $MSC^{intelligent}$

3×10^5 $MSC^{intelligent}$ were cocultured with 2×10^4 Her2 (+) tumor cells (Skov3-GFP, BT474-GFP) for 48 h, and then 50 ng/ml of GCV was added to continually culture for another 12 h, the rupture of $MSC^{intelligent}$ was observed and imaged under a confocal microscope.

2.11. Dynamic record of recognition and rupture of activated $MSC^{intelligent}$

Recognition: 1.5×10^5 $MSC^{intelligent}$ and 1.5×10^5 Skov3-GFP were seeded and cocultured in fibronectin-coated 24 well plates for different time points (15min, 12 h, 24 h, 36 h, 48 h), the cells with fluorescence changes were imaged under a microscope. Simultaneously, the cells were fixed with 4 % PFA and the mCherry-labeled cells were detected by flow cytometry.

Rupture: 1.5×10^5 $MSC^{intelligent}$ and 1.5×10^5 Skov3-GFP were cocultured for 48 h, and 50 ng/ml of GCV was added. Then, the cocultured $MSC^{intelligent}$ and Skov3-GFP were imaged at different time points (0 h, 3 h, 6 h, 9 h, 12 h) under a microscope. Simultaneously, the cells were fixed with 4 % PFA and the mCherry-labeled cells were detected by flow cytometry.

2.12. Living cell workstation

Recognition: 2×10^4 $MSC^{intelligent}$ (10 ppm of CCFCB) and 2×10^4 Skov3-GFP were seeded into the cell culture dish for 6 h, and the cells were imaged under the living cell workstation.

Rupture: 2×10^4 $MSC^{intelligent}$ (10 ppm of CCFCB) and 2×10^4 Skov3-GFP were cocultured for 48 h, and 50 ng/ml of GCV was added. Then, the cocultured $MSC^{intelligent}$ and Skov3-GFP were imaged under the living cell workstation.

2.13. Her2 (+) tumor cell wounds test

When the cultured Skov3-GFP approximately reached 100 % confluence in the cell culture dish, the pipette tip was used to slowly scratch the cell layer, and 2×10^5 $MSC^{intelligent}$ was added to the scratched cell layer.

Recognition: After being cocultured for 24 h, the cells were fixed with 4 % PFA and imaged under confocal microscopy.

Rupture: After being cocultured for 24 h, 50 ng/ml of GCV was added, and the cells were cultured for another 12 h. Then, the cells were fixed with 4 % PFA and imaged under confocal microscopy.

2.14. Treatment of Her2 (+) tumor cells with $MSC^{intelligent}$ in vitro

To determine the killing effect of $MSC^{intelligent}$ (20 ppm of CCFCB) on tumor cells, four groups of cells culture systems were set up, A: Control group, B: $MSC^{intelligent}$ group ($MSC^{intelligent}$:Skov3-GFP = 1:1), C: GCV group, and D: $MSC^{intelligent}$ group + GCV group ($MSC^{intelligent}$:Skov3-GFP = 1:1). Briefly, Skov3-GFP cells was cultured in 96-well plates for 24 h, and $MSC^{intelligent}$ was added and cultured for 48 h; then 50 ng/ml of GCV was added and cultured for 12 h. Centrifuge the culture medium to collect the sediment and resuspend it with fresh medium containing 50 mM hydrogen peroxide with pH = 6.0, then continue to culture for 6 h. The fluorescence intensity of GFP and mCherry in each well was detected by a microplate reader.

2.15. Recognition of Her2 (+) tumor by $MSC^{intelligent}$ in vivo

Lung metastasis model: 3×10^6 Skov3-GFP cells were transplanted into the lungs of BALB/c-nude mice through the tail vein. Skov3-GFP cells were colonized in mouse lung for 3 days, and then 5×10^6 $MSC^{intelligent}$ were transplanted into the mice through the tail vein. In the rupture group, 50 mg/kg of GCV was intravenously injected on Day 5. The lung of mice in each group was isolated and imaged under a stereo fluorescence microscope on Day 7. Then, the lungs were cryosectioned and three-dimensional reconstruction was performed by confocal microscopy to observe the interaction between $MSC^{intelligent}$ and Her2 (+) cells in the lungs.

Solid tumor model: 5×10^6 Skov3-GFP cells were subcutaneously injected into the backside of BALB/c-nude mice for 30 days, and then 5×10^6 $MSC^{intelligent}$ cells were transplanted into the mice through the tail vein at Day 30. In the rupture group, 50 mg/kg of GCV was intravenously injected into the mice on Day 32 and the tumors were harvested on day 34. Then, imaged under confocal microscopy.

2.16. The antitumor effect of $MSC^{intelligent}$ on Her2 (+) tumors in vivo

5×10^6Skov3 cells were injected subcutaneously into the backside of BALB/c-nude mice, and then raised for 30 days. Tumor-bearing mice were randomly divided into four groups: control group, GCV group, $MSC^{intelligent}$ (40 ppm of CCFCB) group, and $MSC^{intelligent}$ (40 ppm of CCFCB) + GCV group. Then, 5×10^6 $MSC^{intelligent}$ were transplanted through the tail vein into the mice of the $MSC^{intelligent}$ group and $MSC^{intelligent}$ + GCV group. After 48 h, 50 mg/kg of GCV was intravenously injected into the mice of the GCV group and $MSC^{intelligent}$ + GCV group and then fed for 21 days. At the end of the experiment, the tumor was isolated and weighed, and the long axis and short axis of the tumor were measured to calculate the tumor volume.

2.17. Statistical analysis

Statistical analysis was performed with the SPSS statistics software. All data were reported as mean ± standard deviation unless specified otherwise. Dunnett's test was used for comparisons among ≥3 groups. $P < 0.05$ was considered to be statistically significant.

3. Results

3.1. Establish an intelligent biomimetic nanoenzymes carrier platform ($MSC^{intelligent}$)

In clinical practice, Her2 protein is a common tumor marker (Fig. 2A), and is found in 20 %–30 % of breast cancers [24], 20 %–30 % of ovarian cancers [25], and 7 %–34 % of gastric cancers [26,27]. To accomplish intelligent modification of the nanoenzymes carrier platform ($MSC^{intelligent}$), enabling it to autonomously and accurately distinguish between Her2 (+) tumors and normal tissue cells, and to achieve precise release of nanoenzymes in Her2 (+) tumors, we

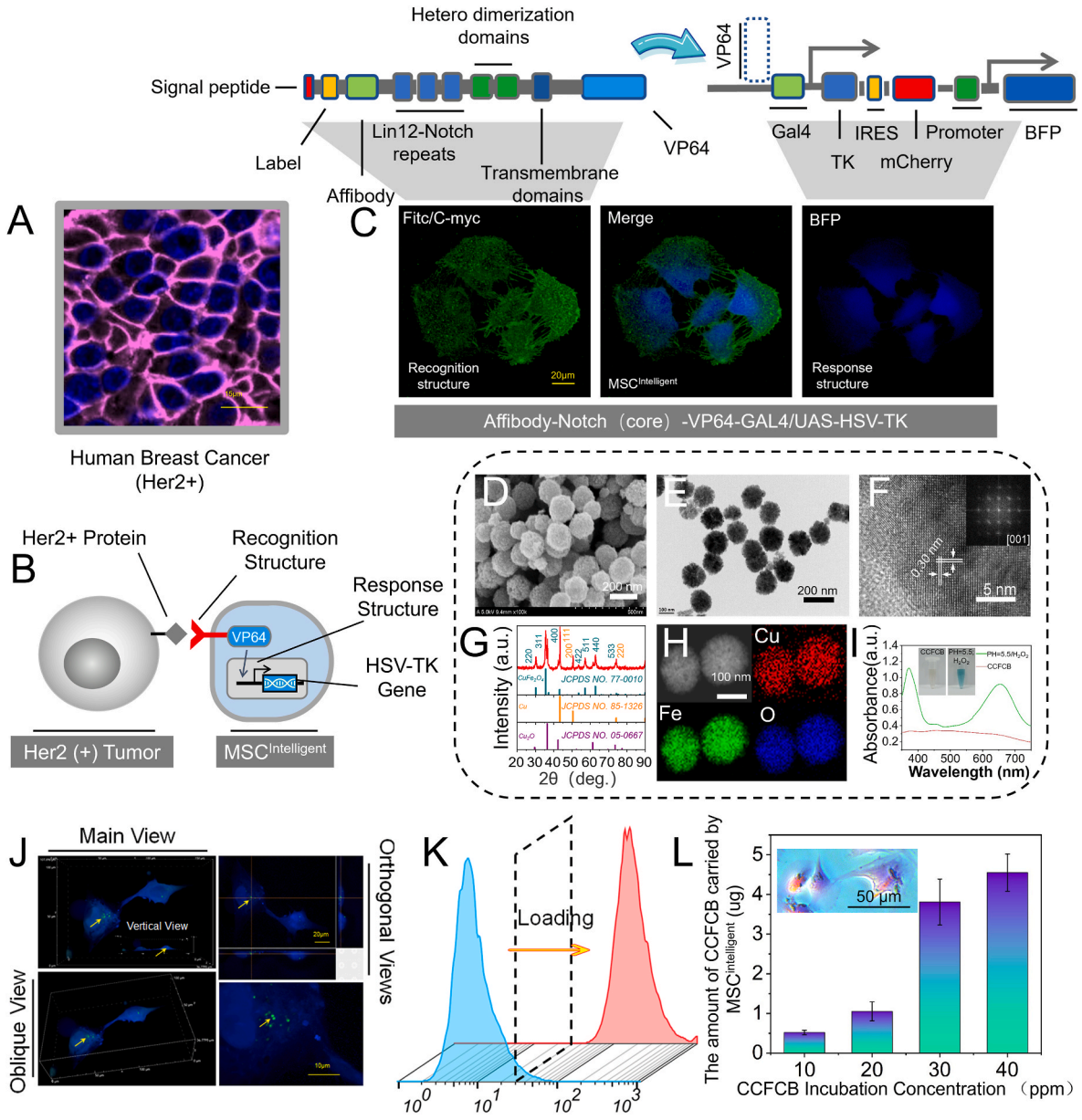

Fig. 2. Design principle of the intelligent modified MSC ^{intelligent} nanoenzymes carrier platform. (A) Human Her2 (+) breast cancer samples. (B) Structure diagram of the MSC^{intelligent} nanoenzymes carrier platform. (C) The recognition structure and response structure diagram of MSC^{intelligent} and immunofluorescence images. Blue and green fluorescence represent the c-myc tag in the recognition structure and BFP in the response structure, respectively. (D) High magnification SEM. (E) TEM and (F) HRTEM images. (G) XRD and (H) EDS mapping images. (I) POD-like activity image of the CCFCB. (J) Z-stack CLSM and (K) flow cytometry demonstrated that MSC^{intelligent} can wrap and load Fitc labeled CCFCB. (L) The amount of CCFCB carried by 1×10^4 MSC^{intelligent}. Insert Prussian blue stain image.

endowed the MSC Affibody Notch (core) - VP64-GAL4/UAS-HSV-TK artificial signaling pathway with gene editing technology. Specifically, the intelligent core of this intelligent biomimetic nanoenzymes carrier platform consists of two parts: a recognition structure (Affibody-Notch (core) -VP64) and a response structure (GAL4/UAS-HSV-TK) (Fig. 2B and C). In the recognition structure, we retained the core domain of the notch protein, replaced the extracellular and intracellular structures of the natural Notch protein with affibody and VP64, respectively, and added a c-myc tag (EQKLISEEDL) and CD8α signal peptide (MALPVTALLLPLALLLHAARP) at the N-terminal of the recognition structure (Fig. 2B and C). In the recognition structure, the affibody connected to the N-terminal of the notch (core) can perceive the Her2 (+) tumor and transmit the recognition signal to VP64. This signal perception and transmission mode depend on our retention of the S3 cleavage site of the natural notch protein in the recognition structure. When the Affibody-Notch (core) recognizes the Her2 protein on the tumor surface, the intracellular γ-secretase will act on the S3 site of the Notch protein, resulting in the disassociation of VP64, which will be transferred into the nucleus and complete the tumor signal transmission. Subsequently, to enable MSC^{intelligent} to provide feedback instructions for rupture and release nanoenzymes after receiving the Her2 (+) tumor stimulation signal, we cloned five copies of the GAL4 DBD targeting sequence (GGAGCACTGTCCTCCGAACG) into the minimal CMV promoter of MSC^{intelligent} to drive the HSV-TK gene and added a BFP label (blue fluorescent protein) to the response structure of the intelligent program (Fig. 2B and C). When the recognition structure of MSC^{intelligent} receives Her2 (+) tumor stimulation, VP64 will transport stimulation signals to the nucleus, where it will combine with the GAL4 DBD target sequence to form an intact GAL4-VP64 transcription activator and further activate the expression of HSV-TK in the response structure. The green and blue

fluorescence in Fig. 2C represent the recognition structure and response structure of $MSC^{intelligent,}$ respectively, which together constitute the artificial signaling pathway of $MSC^{intelligent}$. Through Flow cytometry analysis of intelligently modified $MSC^{intelligent}$ revealed that they still conform to internationally recognized criteria for MSCs, with positive rates exceeding 95 % for CD70, CD90, and CD105, and no expression of CD11b, CD19, CD34, CD45, and HLA-DR (Fig. S1). In the coculture system with hPBMC cells, no significant differences were observed in T cells ($CD3^+$, $CD3^+$ $CD4^+$, and $CD3^+$ $CD8^+$) and B cells ($CD3^-$ $CD19^+$) between the $MSC^{intelligent}$ group and the MSC group, and neither group could activate the immune system (Fig. S2).

In this study, the nanoenzymes in $MSC^{intelligent}$ is CCFCB. First, we used a facile one-step solvothermal reaction to synthesize Cu + -containing Cu/Fe nanoclusters (CCFC) and then oxidized the CCFC in water exposed to air, thus yielding Cu+ with high catalytic activity. The morphology of the CCFC was characterized by scanning electron microscopy (SEM) and transmission electron microscopy (TEM), as presented in Fig. 2D, E and Fig. S3. It could be clearly observed that CCFC consists of uniform sphere-shaped nanocrystal clusters possessing an average diameter of ~150 nm. Fig. 2F displays the high-resolution TEM (HRTEM) image of nanocrystal clusters, in which the marked interplanar d-spacings of ~0.30 nm correspond to the {220} lattice fringes of cubic $CuFe_2O_4$ crystal. Moreover, the diffraction pattern (Fig. 2F, inset) of the fast Fourier transform (FFT) from the HRTEM image can be indexed to the [001] zone axis of the cubic $CuFe_2O_4$ crystal. The crystal structure of CCFC was further verified by X-ray diffraction (XRD). As seen from Fig. 2G, the position and relative intensity of the diffraction peaks coincide well with the data of standard $CuFe_2O_4$ (JCPDS 77–0010), copper (JCPDS 85–1326), and Cu2O (JCPDS 05–0667). Different from previous reports concerning $CuFe_2O_4$, the as-prepared CCFC has a high peroxidase (POD) like catalytic activity of Cu+ from Cu2O, promising as a high-activity nanoenzymes in cancer catalytic therapy. Scanning transmission electron microscopy (STEM) with energy dispersive X-ray spectroscopy (EDS) mapping of the nanocrystal clusters was also recorded, displaying a homogeneous distribution of Cu, Fe, and O elements in the clusters (Fig. 2H). To improve the biocompatibility of CCFC for safe loading into $MSC^{intelligent}$, BSA was modified on the surface of CCFC to ultimately achieve BSA-modified CCFC (CCFCB) nanoenzymes. Ideally, CCFCB nanoenzymes containing high catalytic activity of Cu+ is expected to have excellent POD-like catalytic activity, which can convert hydrogen peroxide (H_2O_2) in the tumor microenvironment into highly active hydroxyl radicals (·OH), thereby destroying the proteins or deoxyribonucleic acid (DNA) of tumor cells and leading to cell apoptosis [28,29]. As expected, our results indicated that CCFCB nanoenzymes exhibited robust POD-like activity under acidic and H_2O_2 conditions, while without acidic and H_2O_2 conditions, there was no obvious change observed in the absorbance of TMB (Fig. 2I). However, the pH value inside the cell is usually neutral, which will prevent the damage of nanoenzymes to $MSC^{intelligent}$. Subsequent CCK-8 (Fig. S4 A), flow cytometry (Fig. S4 B), ROS staining (Fig. S4 C), and live-dead cell staining (Fig. S4 D) results confirmed the promising anti-tumor activity of CCFCB nanoenzymes.

The CCFCB in the $MSC^{intelligent}$ was marked by Fitc. Based on the three-dimensional reconstruction scanning of the confocal microscope, we confirmed that CCFCB existed in the interior of $MSC^{intelligent}$, rather than on the surface of cells (Fig. 2J), which avoids nanoenzymes direct contact with normal tissue cells. Flow cytometry (Fig. 2K), Prussian Blue/phenol red staining (Fig. 2L), and CCFCB content detection (Fig. L, Fig. S5) also demonstrated the CCFCB in $MSC^{intelligent}$ from multiple perspectives.

3.2. $MSC^{intelligent}$ intelligently recognize Her2 (+) tumors

To visually present the signal feedback process of $MSC^{intelligent}$ after recognizing Her2 (+) tumors, we used the IRES structure to connect the mCherry and HSV-TK genes in the response structure (Fig. 2C). Therefore, when $MSC^{intelligent}$ recognizes Her2 (+) tumors, $MSC^{intelligent}$ will initiate the expression of the TK gene accompanied by emitting red fluorescence (activated $MSC^{intelligent}$). As expected, $MSC^{intelligent}$ shows extraordinary recognition ability for Her2 (+) tumor. After coculturing $MSC^{intelligent}$ (blue fluorescence) with two kinds of Her2 (+) tumor cells, Skov3 and BT474 (green fluorescence), $MSC^{intelligent}$ accurately recognized Her2 (+) tumors, that the blue fluorescence-labeled $MSC^{intelligent}$ emitting red fluorescence. The activated $MSC^{intelligent}$ (red fluorescence) that recognized Her2 (+) tumors closely surrounded Her2 (+) tumor cells (green fluorescence), and both exhibited a similar distribution (Fig. 3A). Moreover, in the follow-up Transwell experiment, we found that the intelligent recognition of Her2 (+) tumors by $MSC^{intelligent}$ depended on the direct contact between $MSC^{intelligent}$ and Her2 (+) tumors (Fig. 3B). In three kinds of culture systems, the activated $MSC^{intelligent}$ only appeared in the contact coculture system of $MSC^{intelligent}$ and Her2 (+) tumors, but both $MSC^{intelligent}$ cultured alone or noncontact cocultured with Her2 (+) tumors could not be activated (Fig. 3B). Consistent conclusions were reached when analyzing the fluorescence intensity of $MSC^{intelligent}$-Her2 (+) tumor coculture systems. Three peaks are shown in Fig. S6: the green, blue, and red peaks represent Her2 (+) tumors, total $MSC^{intelligent}$, and activated $MSC^{intelligent}$, respectively. The results indicated that among the four blue peaks, only two blue peaks adjacent to the green peak turned red, demonstrating that the recognition of Her2 (+) tumors by $MSC^{intelligent}$ depended on direct contact with Her2 (+) tumors (Fig. S6). Based on the three-dimensional reconstruction, we also found direct contact between $MSC^{intelligent}$ and Her2 (+) tumors in three-dimensional space (Fig. 3C). This contact recognition mode between $MSC^{intelligent}$ and Her2 (+) tumors ensures the activation of $MSC^{intelligent}$ only at the tumor site and avoids $MSC^{intelligent}$ activation at the nontumor site. Simultaneously, we also detected activated $MSC^{intelligent}$ by flow cytometry in the $MSC^{intelligent}$ and Her2 (+) tumor coculture system, strongly confirming the capacity to recognize Her2 (+) tumors by $MSC^{intelligent}$ (Fig. S7). Furthermore, to dynamically observe the process of $MSC^{intelligent}$ recognition of Her2 (+) tumors, we performed live-cell workstation imaging. Conclusively, these results revealed that the intelligent recognition of Her2 (+) tumors by $MSC^{intelligent}$ can be divided into four stages: preparation, approach, contact, and activation (Fig. 3D, video 1). Additionally, the recognition of $MSC^{intelligent}$ for Her2 (+) tumor is a sensitive process. $MSC^{intelligent}$ only needs a pseudopodium to contact the Her2 (+) tumor to fully complete the recognition and signal feedback to the Her2 (+) tumor (activate the downstream HSV-TK gene and turn red), and $MSC^{intelligent}$ without contact with Her2 (+) tumors will not be activated (Fig. S8, video 2). To detect the peak time when $MSC^{intelligent}$ fed back the HSV-TK gene after recognizing the Her2 (+) tumor. We discovered that $MSC^{intelligent}$ could be completely activated within 36 h after recognizing Her2 (+) tumors by evaluating the red fluorescence intensity in the $MSC^{intelligent}$-Her2 (+) tumor coculture system through confocal microscopy and flow cytometry (Fig. 3E and S9).

Supplementary video related to this article can be found at https://doi.org/10.1016/j.mtbio.2024.101105

Video 1. 2

To further testify to the accuracy of $MSC^{intelligent}$ in recognizing Her2 (+) tumors from a macroscopic view. We divided the tumor area (treatment area) and the nontumor area (safety area) at the cellular level through the Her2(+) tumor wound test, and $MSC^{intelligent}$ was then seeded into the tumor cell layer to initiate the recognition process of $MSC^{intelligent}$ to Her2 (+) tumors in vitro. Satisfactorily, the results demonstrated that $MSC^{intelligent}$ can accurately recognize the Her2 (+) tumor area even on a large scale, and the activated $MSC^{intelligent}$ perfectly overlaps with the tumor to form a treatment area, but no phenomenon of existing activated $MSC^{intelligent}$ (red fluorescence) in the nontumor area was observed (Fig. 3F). Subsequently, to further confirm the accuracy of $MSC^{intelligent}$ recognition, two kinds of Her2 (+) tumor cells (Skov3 and BT474) and four kinds of normal human tissue cells

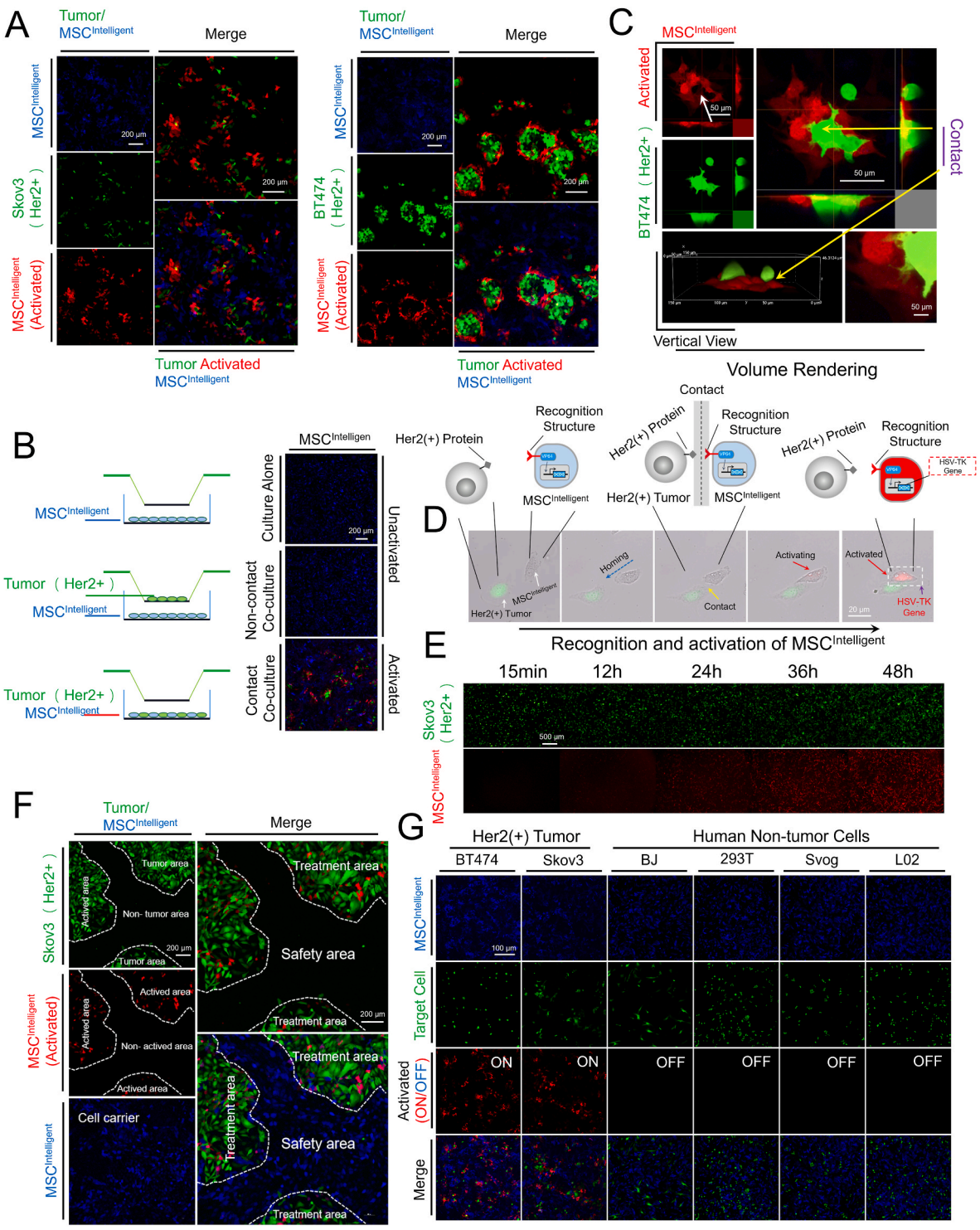

Fig. 3. MSC^{intelligent} intelligence recognizes/distinguishes Her2 (+) tumor and normal tissue cells. (A) MSC^{intelligent} cells were cocultured with Skov3 and BT474 cells. Green cells are Her2 (+) tumor cells, blue cells are MSC^{intelligent}, and red cells are MSC^{intelligent} that recognize Her2 (+) tumor cells. (B) The contact and noncontact coculture systems between MSC^{intelligent} and Her2 (+) tumor cells were established by Transwell assays. (C) Z-stack CLSM image of MSC^{intelligent}-Her2 (+) tumor cells. (D) Dynamic recognition process of Her2 (+) tumors by MSC^{intelligent}. (E) The red fluorescence intensity of activated MSC^{intelligent} at different time points in the coculture system of MSC^{intelligent} and Skov3 cells. (F) MSC^{intelligent} and Skov3 cell wounds were cocultured for 24 h. (G) MSC^{intelligent} cells cocultured with four kinds of normal tissue cells and two kinds of Her2 (+) tumor cells. Red cells are MSC^{intelligent} that recognizes Her2 (+) tumor cells.

(kidney: 293 T; liver: L02; skin: BJ and ovary: Svog) were selected for coculture with MSC^{intelligent} cells. Consistent with the expected results, MSC^{intelligent} was exclusively activated by two kinds of Her2 (+) tumor cells in six groups of coculture systems, while four normal human cells were unable to activate MSC^{intelligent} (Fig. 3G). Consequently, the aforementioned findings demonstrated both the accuracy of recognition of Her2 (+) tumors and the intelligence of artificial signaling pathway equipped in MSC^{intelligent}.

3.3. MSC^{intelligent} controllably releases nanoenzymes

GCV is widely used in treating herpes simplex and is characterized by low toxicity and affordable price. Under the catalysis of HSV-TK, GCV can be transformed into GCV triphosphate, which interferes with DNA synthesis and leads to the rupture of cells. According to this principle, in this study, to make the process of nanoenzymes release by MSC^{intelligent} controllable, we endowed MSCs with the ability to recognize the feedback HSV-TK gene after Her2(+) tumors. Due to the lack of a Her2 signal in normal tissue cells, MSC^{intelligent} will not activate the HSV-TK gene. Therefore, because of the difference in the expression of the HSV-TK gene of MSC^{intelligent} in tumor sites and normal tissues, MSC^{intelligent} will be ruptured in tumor sites under the mediation of GCV but still remain intact in nontumor sites, resulting in the accurate release of nanoenzymes in tumor sites. Next, to validate the process of GCV-mediated nanoenzymes release, two kinds of Her2 (+) tumors were selected to be cocultured with MSC^{intelligent} for 48 h, and then, GCV was added for 12 h. The results demonstrated that GCV can accurately rupture the activated MSC^{intelligent} near the tumor, and the ruptured MSC^{intelligent} fragments closely surrounded the Her2 (+) tumor, and both showed a distribution similar to the tumor (Fig. 4A). Additionally, based on the three-dimensional reconstruction of the confocal microscope, we confirmed that the activated MSC^{intelligent} was ruptured and the potential of nanoenzymes was released around the Her2 (+) tumor. Consistent with the findings in Fig. 4A, the MSC^{intelligent} (blue fluorescence) that could not recognize the tumor remained intact, and the preloaded nanoenzymes could not be released even under the mediation of GCV due to the unactivation of HSV-TK expression in MSC^{intelligent} (Fig. 4B). The same result was revealed in the subsequent flow cytometry results and GCV toxicity results. The MSC^{intelligent} which represents a recognized tumor, after adding GCV the activation peak disappeared (Fig. 4C). GCV showed significant cytotoxicity towards only activated MSCintelligent (Fig. S10). Then, we dynamically observed the rupture process of activated MSC^{intelligent} in the presence of GCV through the living cell workstation (Fig. 4D, video 3). To further validate the accuracy and safety of MSC^{intelligent} in the treatment process, GCV was added to the cocultured MSC^{intelligent} with a scratched tumor cell layer for another 12 h. As expected, after GCV addition, the activated MSC^{intelligent} in the tumor area (MSC^{intelligent} treatment area) was completely ruptured and died. However, in the nontumor area, MSC^{intelligent}

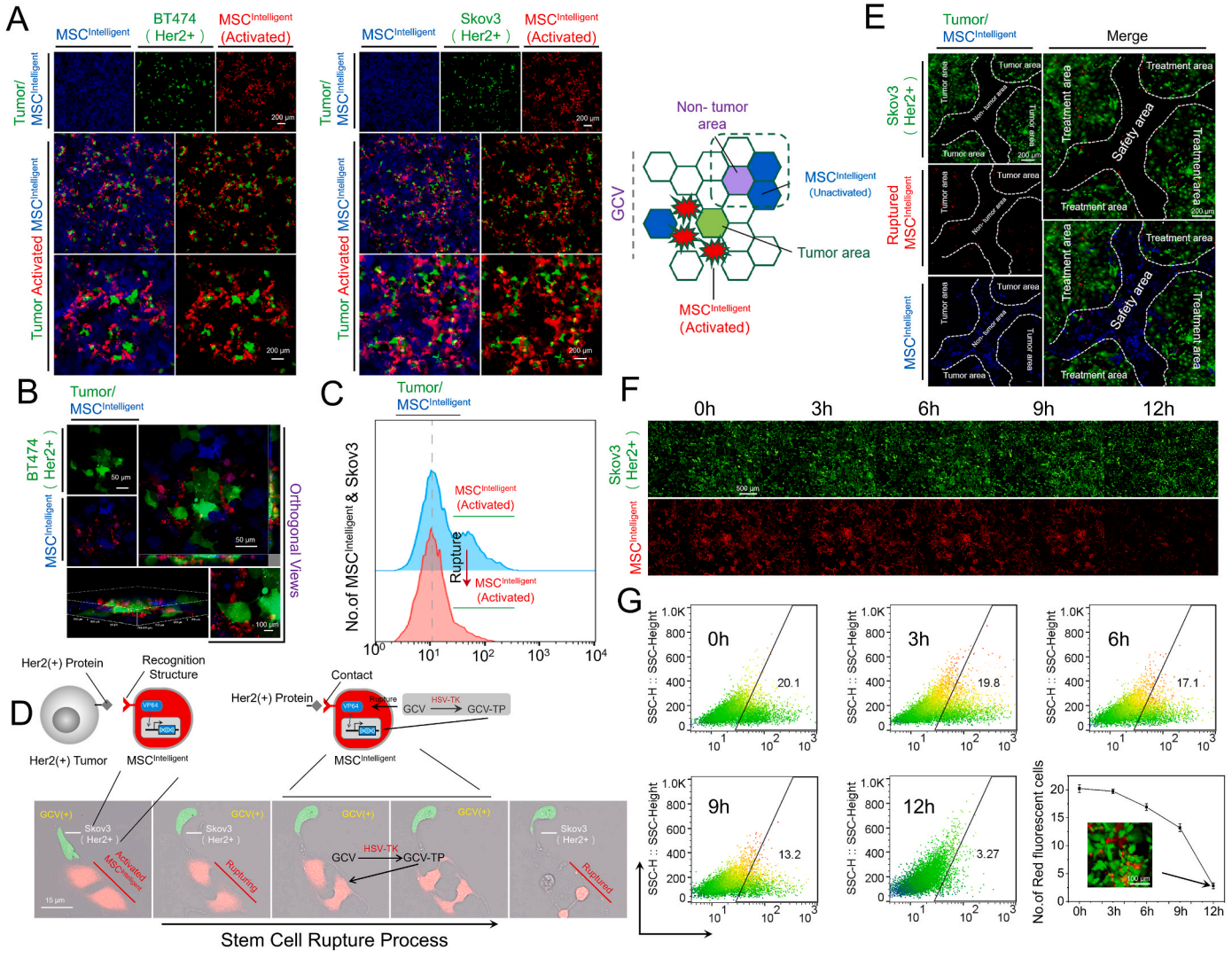

Fig. 4. GCV mediates the precise nanoenzymes release of MSC^{intelligent}. (A) After MSC^{intelligent} recognized Her2 (+) tumor cells (Skov3 and BT474), GCV was added to induce nanoenzymes release. The red cell fragments are activated MSC^{intelligent}, and the green cells are Her2 (+) tumor cells. (B) Activated MSC^{intelligent} accurate rupture Z-stack CLSM image and (C) flow cytometry results. (D) The dynamic rupture process of activated MSC^{intelligent} after adding GCV. (E) In Skov3 cell wounds, after MSC^{intelligent} recognition of Skov3 cells, GCV was added and cultured for 24 h. (F) MSC^{intelligent} red fluorescence intensity images and (G) flow cytometry results of activated MSC^{intelligent} at different time points after GCV was added to the coculture system of MSC^{intelligent} and Skov3 cells.

remained unactivated and unresponsive to GCV, and the unactivated MSC^{intelligent} was perfectly complementary to the tumor area and overlapped with the scratched area (safe area, Fig. 4E). These results demonstrated the accuracy of nanoenzymes release in MSC^{intelligent} mediated by GCV. Finally, in order to calculate the complete rupture time of activated MSC^{intelligent} in the presence of GCV, we observed the change of red fluorescence of activated MSC^{intelligent} and further confirmed by flow cytometry, the results indicated that GCV could completely rupture the activated MSC^{intelligent} within 12 h (Fig. 4F and G).

Supplementary video related to this article can be found at https://doi.org/10.1016/j.mtbio.2024.101105

Video 2. 3

Video 3. 4

3.4. Recognition and inhibition of Her2 (+) tumors by MSC^{intelligent} in vivo

To evaluate the capacity of MSC^{intelligent} to recognize Her2 (+) tumors in vivo, we respectively established a lung metastasis model and solid tumor model of Her2 (+) tumors. In the lung metastasis model, we found that MSC^{intelligent} could still accurately recognize Her2 (+) tumors in lung tissue based on observing red fluorescence under a stereo fluorescence microscope (Fig. 5A). Subsequently, the activated MSC^{intelligent} could be successfully ruptured after GCV injection and completed the release of the nanoenzymes (Fig. 5B). The following results of three-dimensional reconstruction of lung slices under confocal microscopy confirmed that MSC^{intelligent} was capable of accurately distinguishing Her2 (+) tumor and normal tissue cells in vivo. Consistent with the results in vitro, the MSC^{intelligent} that recognized the Her2 (+) tumor was activated (red fluorescence), while the MSC^{intelligent} that did not recognize the Her2 (+) tumor remained unactivated (blue fluorescence) in the lung tissue (Fig. 5C). Simultaneously, in the solid Her2 (+) tumor model, MSC^{intelligent} could migrate into the tumor site after being transplanted into mice via the tail vein and further accomplish the recognition of Her2 (+) tumors and that release of nanoenzymes under the mediation of GCV (Fig. 5D). Promisingly, the antitumor activity of MSC^{intelligent} was further confirmed under a confocal microscope, and we observed that

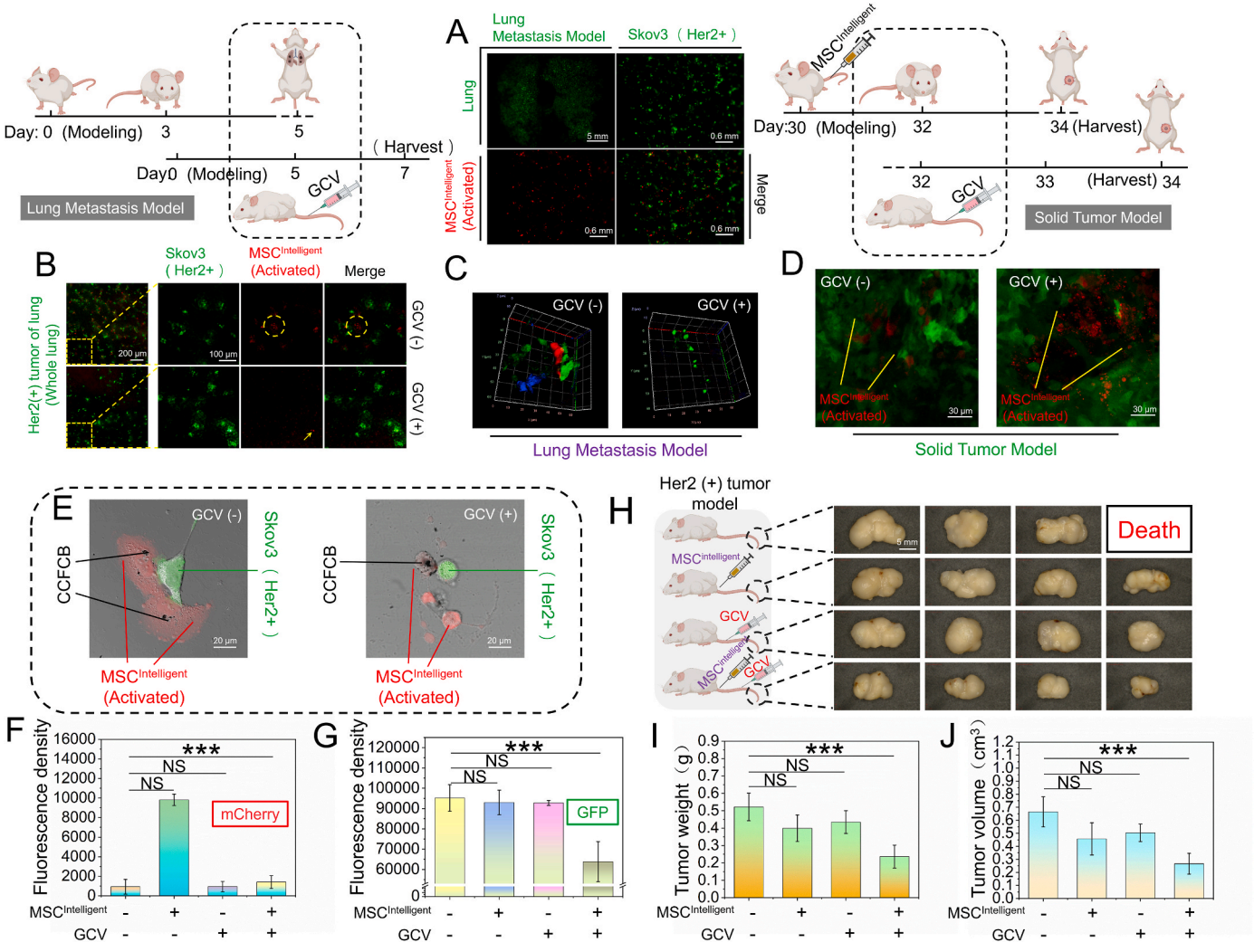

Fig. 5. Intelligent recognition and antitumor effect of the MSC^{intelligent} nanoenzymes carrier platform on Her2 (+) tumors. (A) The recognition of Her2 (+) tumors by the MSC^{intelligent} nanoenzymes carrier platform in the whole lung. The image in the upper left is the macroscopic result observed under a stereo fluorescence microscope, while the images in the lower left, upper right, and lower right are the locally magnified results. (B) High magnification fluorescence imaging of (A). (C) Z-stack CLSM image of lung section of (B). Green cells are Her2 (+) tumor cells, blue cells are MSC^{intelligent}, and red cells are MSC^{intelligent} that recognize Her2 (+) tumor cells. (D) Intelligent recognition of Her2 (+) tumors by MSC^{intelligent} in the solid tumor model. (E) Bright-field image of CCFCB/MSC^{intelligent} anti Her2 (+) tumor (Skov3). (F, G) Microplate reader detection of recognition and anti-tumor effects of CCFCB/MSC^{intelligent} on Her2 (+) tumors. Red fluorescence (mCherry) represents activated MSC^{intelligent}; Green fluorescence (GFP) represents Skov3 cells. (H) Images of Her2 (+) tumor-bearing mice and tumors and (I) tumor weight and (J) volume after treatment.

GCV-mediated release of CCFCB in MSC^{intelligent} efficiently induced the death of Her2 (+) tumor cells (Skov3) in vitro (Fig. 5E). Then, four groups of cell culture systems were set up, A: Control group, B: MSC^{intelligent} group, C: GCV group, and D: MSC^{intelligent} group + GCV group, and the fluorescence intensity of mCherry (activated MSC^{intelligent}) and GFP (Her2 (+) tumor) were measured in each group. Because the rupture of activated MSC^{intelligent} under the mediation of GCV in Group D resulted in the loss of red fluorescence, we only detected intense red fluorescence in Group B (Fig. 5F). Consistent with the above findings, CCFCB in MSC^{intelligent} could be successfully released and perform its antitumor effect only in Group D (Fig. 5G). Moreover, loading different concentrations of CCFCB in MSC^{intelligent} can also enhance their antitumor activity, which was validated in CCK-8 (Fig. S11 A), Skov3-GFP fluorescence imaging (Fig. S11 B), and Skov3-GFP fluorescence intensity detection (Fig. S11C). Simultaneously, In the mouse model, as anticipated, there was a significant reduction in both tumor weight and volume following treatment with MSC^{intelligent} (Fig. 5H–J). To verify the safety of MSC^{intelligent}, we conducted liver and kidney function testing, HE staining, and immunological analysis on MSC^{intelligent} group and MSC^{intelligent} + GCV group mice, respectively. The results showed that neither MSC^{intelligent} nor MSC^{intelligent} + GCV can cause liver and kidney toxicity(Fig. S12). No organic lesions caused by MSC^{intelligent} and MSC^{intelligent} + GCV were found in the slices of the liver, spleen, kidneys, heart, pancreas, and lungs (Fig. S13). Furthermore, MSC^{intelligent} and MSC^{intelligent} + GCV can not cause significant immune system abnormalities. There were no significant differences observed in $CD3^+$, $CD3^+CD4^+$, $CD3^+CD8^+$, and $CD3^-CD19^+$ cells in mice transplanted with MSC^{intelligent} and MSC^{intelligent} + GCV (Fig. S14), which is mutually confirmed with Fig. S2.

4. Discussion

Nanoenzymes administered systemically often results in undesirable side effects and toxicity owing to their accumulation in non-tumor sites and the lack of drug selectivity [9,10,30]. Therefore, there is a substantial need for nanoenzymes delivery systems that can exclusively release nanoenzymes at tumor sites to decrease unwanted side effects and improve efficacy. The primary goal of this study was to develop a biomimetic nanoenzymes carrier platform with "wisdom", which can intelligently distinguish tumor cells from normal tissue cells, and accurately release nanoenzymes at tumor sites. Promisingly, our intelligent design concept endows MSC^{intelligent} with an extraordinary recognition capacity for tumors (Fig. 3A–F, and Fig. 5C and D). Its unique recognition structure and reflection structure can receive tumor signals and transform them into HSV-TK gene expression behavior (Fig. 2C). Subsequently, under the action of GCV, the MSC^{intelligent} that recognizes the tumor will rupture and accurately release nanoenzymes at the tumor site.

The intelligence of MSC^{intelligent} possesses several distinct features over traditional biomimetic nanoenzymes carrier platform such as cells, bacteria, and CAR-T. First, the chemotaxis of cells and bacteria carrier platforms to tumors depends on the recognition of chemokine released from the tumor by chemokine receptors on the cell surface [11,31]. However, the original role of these chemokine receptors is not to receive tumor signals. Therefore, they could not accurately distinguish whether chemokines derived from the tumor or inflammatory location. Which is just an idealized and rough combination between tumors and carrier platforms. But the stimulus source and feedback behavior of MSC^{intelligent} are customized through artificial signaling pathway, which endows MSC^{intelligent} 's behavior more explicit and predictable. Moreover, unlike traditional targeting strategies that increase local drug concentration, an intelligent biomimetic nanoenzyme carrier platform has preliminary "wisdom", which can autonomously identify lesions and make the nanoenzyme only release/act on the tumor site. Second, although the CAR-T carrier platform can also couple the designated disease antigen signal with the synthesis of a natural T cell activation program [23,32,33]. However, its tumor binding mode is more similar to antigen binding to antibody. Hinge region and transmembrane domain only play the role of overcome steric hindrance and membrane localization, which cannot transmit tumor signals [33,34]. CAR-T change only the INPUT that the cell senses, the OUTPUT is still the full T cell activation program [23]. Whether antigen binding domain recognizes to tumor does not affect the behavior of CART, CART remains in the activated state even in normal tissue. In contrast, MSC^{intelligent} is a nanoenzymes carrier platform with artificial intelligence, which can recognize and transform tumor signals into HSV-TK gene expression behavior (Fig. 2C). There is a logical connection between tumor signal and the behavior of MSC^{intelligent}, which ensure that the behavior of MSC^{intelligent} to feedback HSV-TK gene expression and nanoenzymes release nanoenzymes will exclusively occur at the tumor site. Finally, the intelligent program of MSC^{intelligent} is replaceable. Therefore, we can replace the tumor type recognized by MSC^{intelligent} and coupled feedback signals by replacing the Affibody-Notch(core) sequence in the recognition structure or the GAL4/UAS-HSV-TK sequence in the response structure. For example, replacing Affibody-Notch(core) with (PD-1, CTLA-4, CD19)-Affibody--Notch(core) enables MSC^{intelligent} to recognize PD-1, CTLA-4, and CD19 positive tumors; Or replacing GAL4/UAS-HSV-TK with GAL4/UAS-(Glutathione Peroxidase) enable MSC^{intelligent} to feedback glutathione peroxidase expression which enhances the antitumor effect of the nanoenzymes after recognizing the tumor signal.

In addition, the greatest challenge of the cell, bacteria, CAR-T carrier platforms is that the loaded nanoenzymes cannot be efficiently released after being transported to tumors, which may block the contact between nanoenzymes and tumor cells or tumor microenvironment and further impair the anti-tumor effects of nanoenzymes [11,12,31,32]. However, the intelligent program in MSC^{intelligent} can convert tumor signals into HSV-TK expression, and then under the action of GCV, the MSC^{intelligent} after recognizing tumors will be ruptured and nanoenzymes released. While in non-tumor sites, HSV-TK expression will not be initiated due to the unactivation of artificial signaling pathways in MSC^{intelligent}, resulting in the unresponsiveness of MSC^{intelligent} to GCV and inhibition of nanoenzymes release (Fig. 4A, B, and E). Consequently, MSC^{intelligent} can not only effectively block the contact between nanoenzymes and normal tissue, but also realize the precise release of nanoenzymes in the tumor site. It is noteworthy that, despite undergoing intelligent modification, MSC^{intelligent} still adheres to the internationally recognized standards for MSCs (Fig. S1). This establishes the groundwork for MSC^{intelligent} to continue maintaining the original low immunogenicity of MSCs (Fig. S2), which can prevent nanoenzyme leakage caused by immune system attacks on MSC^{intelligent}. In contrast, exogenous biomimetic platforms, such as bacteria, with high immunogenicity may lead to abnormal release of nanoenzymes.

In this study, CCFCB/MSC^{intelligent} and Her2 (+) tumors are taken as examples to preliminarily demonstrate the intelligence of artificial signaling pathway in MSC^{intelligent}. But the anti-tumor strength of MSC^{intelligent} depends on the loaded nanoenzymes. We can change the anti-tumor ability of MSC^{intelligent} by changing the type of nanoenzymes. And we hope that this intelligent program can be synergetically developed with various nanoenzymes in the future studies. Once a nanoenzymes that can cooperate with MSC^{intelligent} feedback signal is developed, the anti-tumor effect of nanoenzymes/MSC^{intelligent} will be further exerted. For example, the nanoenzymes can switch between toxic and non-toxic by interacting with the feedback signal in MSC^{intelligent}, so that nanozymes can exert toxicity only at the tumor site. Overall, the intelligent biomimetic nanoenzymes carrier platform constructed by introducing artificial signaling pathway is a new design concept, which opens up a new direction for nanoenzymes-based tumor therapy.

CRediT authorship contribution statement

Yuliang Sun: Writing – review & editing, Writing – original draft,

Software, Methodology, Investigation, Data curation, Conceptualization. **Wenlong Zhang:** Software, Project administration, Investigation, Data curation. **Yilin Lu:** Formal analysis, Data curation. **Yanan He:** Software, Project administration, Data curation. **Badrul Yahaya:** Writing – review & editing, Writing – original draft, Supervision, Software, Data curation. **Yanli Liu:** Methodology, Formal analysis, Data curation. **Juntang Lin:** Writing – review & editing, Writing – original draft, Validation, Supervision, Software, Formal analysis, Data curation, Conceptualization.

Declaration of competing interest

The authors declare that they have no known competing financial interests or personal relationships that could have appeared to influence the work reported in this paper.

Data availability

Data will be made available on request.

Acknowledgements

This work was supported by the Science and Technology Tackling Key Project of Henan Province (222102310103) and Natural science Foundation of Henan Province(242300421199 and 235101610002).

Appendix A. Supplementary data

Supplementary data to this article can be found online at https://doi.org/10.1016/j.mtbio.2024.101105.

Abbreviations

MSCs	Mesenchymal stem cell
$MSC^{intelligent}$	Intelligent biomimetic nanoenzymes carrier platform
Matrix metalloproteinase-2	Mmp-2
Matrix metalloproteinase-9	Mmp-9
L02	Human normal liver cell
293 T	Human renal epithelial cells
BJ	Human skin fibroblasts
Svog	Ovarian granulosa cells
BT474	Human breast ductal carcinoma cells
Skov3	Human ovarian cancer cells

References

[1] S. Wang, J. Mao, H. Liu, S. Huang, J. Cai, W. Gui, J. Wu, J. Xu, J. Shen, Z. Wang, pH-Sensitive nanotheranostics for dual-modality imaging guided nanoenzyme catalysis therapy and phototherapy, J. Mater. Chem. B 8 (22) (2020) 4859–4869.
[2] M. Lyu, D. Zhu, X. Kong, Y. Yang, S. Ding, Y. Zhou, H. Quan, Y. Duo, Z. Bao, Glutathione-depleting nanoenzyme and glucose oxidase combination for hypoxia modulation and radiotherapy enhancement, Adv. Healthcare Mater. 9 (11) (2020) e1901819.
[3] Y. Chen, Y. Cai, X. Yu, H. Xiao, H. He, Z. Xiao, Y. Wang, X. Shuai, A photo and tumor microenvironment activated nano-enzyme with enhanced ROS generation and hypoxia relief for efficient cancer therapy, J. Mater. Chem. B 9 (39) (2021) 8253–8262.
[4] W. Du, T. Liu, F. Xue, X. Cai, Q. Chen, Y. Zheng, H. Chen, Fe(3)O(4) mesocrystals with distinctive magnetothermal and nanoenzyme activity enabling self-reinforcing synergistic cancer therapy, ACS Appl. Mater. Interfaces 12 (17) (2020) 19285–19294.
[5] Z. Zeng, C. Zhang, J. Li, D. Cui, Y. Jiang, K. Pu, Activatable polymer nanoenzymes for photodynamic immunometabolic cancer therapy, Adv. Mater. 33 (4) (2021) e2007247.
[6] M. Chang, Z. Hou, M. Wang, C. Yang, R. Wang, F. Li, D. Liu, T. Peng, C. Li, J. Lin, Single-atom Pd nanozyme for ferroptosis-boosted mild-temperature photothermal therapy, Angew Chem. Int. Ed. Engl. 60 (23) (2021) 12971–12979.
[7] T. Lammers, F. Kiessling, M. Ashford, W. Hennink, D. Crommelin, G. Storm, Cancer nanomedicine: is targeting our target? Nat. Rev. Mater. 1 (9) (2016).
[8] M. Torrice, Does nanomedicine have a delivery problem? ACS Cent. Sci. 2 (7) (2016) 434–437.
[9] G. Yang, S.Z.F. Phua, A.K. Bindra, Y. Zhao, Degradability and clearance of inorganic nanoparticles for biomedical applications, Adv. Mater. 31 (10) (2019) e1805730.
[10] M. Yu, J. Zheng, Clearance pathways and tumor targeting of imaging nanoparticles, ACS Nano 9 (7) (2015) 6655–6674.
[11] Y. Zheng, Y. Han, Q. Sun, Z. Li, Harnessing anti-tumor and tumor-tropism functions of macrophages via nanotechnology for tumor immunotherapy, Exploration (Beijing) 2 (3) (2022) 20210166.
[12] C. Gao, Q. Wang, J. Li, C.H.T. Kwong, J. Wei, B. Xie, S. Lu, S.M.Y. Lee, R. Wang, In vivo hitchhiking of immune cells by intracellular self-assembly of bacteria-mimetic nanomedicine for targeted therapy of melanoma, Sci. Adv. 8 (19) (2022) eabn1805.
[13] C. Gao, Z. Lin, B. Jurado-Sanchez, X. Lin, Z. Wu, Q. He, Stem cell membrane-coated nanogels for highly efficient in vivo tumor targeted drug delivery, Small 12 (30) (2016) 4056–4062.
[14] C. Gao, Z. Lin, D. Wang, Z. Wu, H. Xie, Q. He, Red blood cell-mimicking micromotor for active photodynamic cancer therapy, ACS Appl. Mater. Interfaces 11 (26) (2019) 23392–23400.
[15] M. Xuan, J. Shao, L. Dai, J. Li, Q. He, Macrophage cell membrane camouflaged Au nanoshells for in vivo prolonged circulation life and enhanced cancer photothermal therapy, ACS Appl. Mater. Interfaces 8 (15) (2016) 9610–9618.
[16] Y. Liu, R. Niu, F. Yang, Y. Yan, S. Liang, Y. Sun, P. Shen, J. Lin, Biological characteristics of human menstrual blood-derived endometrial stem cells, J. Cell Mol. Med. 22 (3) (2018) 1627–1639.
[17] X. Meng, T.E. Ichim, J. Zhong, A. Rogers, Z. Yin, J. Jackson, H. Wang, W. Ge, V. Bogin, K.W. Chan, B. Thebaud, N.H. Riordan, Endometrial regenerative cells: a novel stem cell population, J. Transl. Med. 5 (2007) 57.
[18] Y. Xu, H. Zhu, D. Zhao, J. Tan, Endometrial stem cells: clinical application and pathological roles, Int. J. Clin. Exp. Med. 8 (12) (2015) 22039–22044.
[19] C.S. Nowell, F. Radtke, Notch as a tumour suppressor, Nat. Rev. Cancer 17 (3) (2017) 145–159.
[20] M. Lecourtois, F. Schweisguth, Indirect evidence for Delta-dependent intracellular processing of notch in Drosophila embryos, Curr. Biol. 8 (13) (1998) 771–774.
[21] G. Struhl, A. Adachi, Nuclear access and action of notch in vivo, Cell 93 (4) (1998) 649–660.
[22] W.R. Gordon, B. Zimmerman, L. He, L.J. Miles, J. Huang, K. Tiyanont, D. G. McArthur, J.C. Aster, N. Perrimon, J.J. Loparo, S.C. Blacklow, Mechanical allostery: evidence for a force requirement in the proteolytic activation of notch, Dev. Cell 33 (6) (2015) 729–736.
[23] L. Morsut, K.T. Roybal, X. Xiong, R.M. Gordley, S.M. Coyle, M. Thomson, W.A. Lim, Engineering customized cell sensing and response behaviors using synthetic notch receptors, Cell 164 (4) (2016) 780–791.
[24] Z. Mitri, T. Constantine, R. O'Regan, The HER2 receptor in breast cancer: pathophysiology, clinical use, and new advances in therapy, Chemother Res Pract 2012 (2012) 743193.
[25] Y. Wu, R.A. Soslow, D.S. Marshall, M. Leitao, B. Chen, Her-2/neu expression and amplification in early stage ovarian surface epithelial neoplasms, Gynecol. Oncol. 95 (3) (2004) 570–575.
[26] J. Ruschoff, W. Hanna, M. Bilous, M. Hofmann, R.Y. Osamura, F. Penault-Llorca, M. van de Vijver, G. Viale, HER2 testing in gastric cancer: a practical approach, Mod. Pathol. 25 (5) (2012) 637–650.
[27] Y.J. Bang, E. Van Cutsem, A. Feyereislova, H.C. Chung, L. Shen, A. Sawaki, F. Lordick, A. Ohtsu, Y. Omuro, T. Satoh, G. Aprile, E. Kulikov, J. Hill, M. Lehle, J. Ruschoff, Y.K. Kang, G.A.T.I. To, Trastuzumab in combination with chemotherapy versus chemotherapy alone for treatment of HER2-positive advanced gastric or gastro-oesophageal junction cancer (ToGA): a phase 3, open-label, randomised controlled trial, Lancet 376 (9742) (2010) 687–697.
[28] X. Zhang, X. Chen, Y. Zhao, Nanozymes: versatile platforms for cancer diagnosis and therapy, Nano-Micro Lett. 14 (1) (2022) 95.
[29] R. Xiong, X. Zhu, J. Zhao, G. Ling, P. Zhang, Nanozymes-mediated cascade reaction system for tumor-specific diagnosis and targeted therapy, Small Methods (2024) e2301676.
[30] J. Wolfram, M. Zhu, Y. Yang, J. Shen, E. Gentile, D. Paolino, M. Fresta, G. Nie, C. Chen, H. Shen, M. Ferrari, Y. Zhao, Safety of nanoparticles in medicine, Curr. Drug Targets 16 (14) (2015) 1671–1681.
[31] H. Wang, C.N. Alarcon, B. Liu, F. Watson, S. Searles, C.K. Lee, J. Keys, W. Pi, D. Allen, J. Lammerding, J.D. Bui, R.L. Klemke, Genetically engineered and enucleated human mesenchymal stromal cells for the targeted delivery of therapeutics to diseased tissue, Nat. Biomed. Eng. 6 (7) (2022) 882–897.
[32] T.T. Smith, S.B. Stephan, H.F. Moffett, L.E. McKnight, W. Ji, D. Reiman, E. Bonagofski, M.E. Wohlfahrt, S.P.S. Pillai, M.T. Stephan, In situ programming of leukaemia-specific T cells using synthetic DNA nanocarriers, Nat. Nanotechnol. 12 (8) (2017) 813–820.
[33] R.C. Sterner, R.M. Sterner, CAR-T cell therapy: current limitations and potential strategies, Blood Cancer J. 11 (4) (2021) 69.
[34] J.N. Brudno, J.N. Kochenderfer, Recent advances in CAR T-cell toxicity: mechanisms, manifestations and management, Blood Rev. 34 (2019) 45–55.